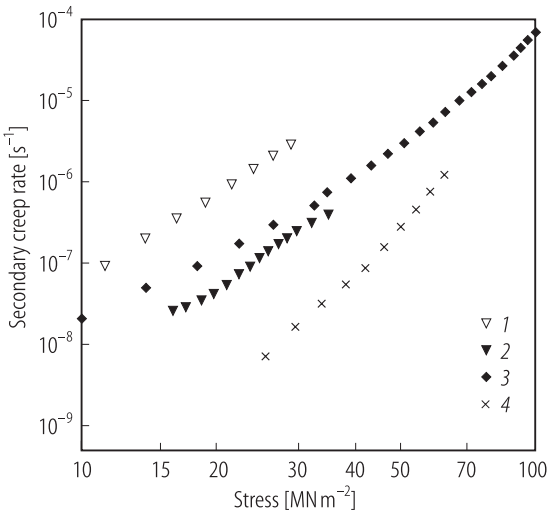

Fig. 19. Stress dependence of the secondary creep rate of Fe_3AlC with αFe precipitate at 950 °C (*1*), Fe_3AlC with graphite at 1000 °C (*2*), $(Ni_{0.8}Fe_{0.2})Al$ at 1027 °C (*3*), and $(Co_{0.8}Ni_{0.2})Al$ at 1027 °C (*4*) [87J1].

Ni–Hf–Al

The microstructure and mechanical properties of several Ni–Al–Hf samples have been studied in the compositional range (NiAl) (β) and Ni_2HfAl (Heusler phase). The volume fraction V_f of the Heusler phase varies from 15 % to 96 %. The yield strength increases with increasing V_f at all temperatures up to 1000 °C. All the alloys can be extensively deformed without fracture at 1000 °C. The hardness of the Heusler alloy is very high (8.3 GPa) at room temperature but slowly decreases up to 600 °C and then rapidly falls off. The brittleness and high hardness at low temperatures is related to lattice distortions.

Table 3. Phases present, lattice parameter *a* and volume fraction of Heusler phase, V_f, in HH-1, HH-2 and HH-4 [90T3].

Alloy	Phase present	*a* [Å]	V_f [%]
HH-1	B2	2.886	14.7
	$L2_1$	6.070	
HH-2	B2	2.885	47.9
	$L2_1$	6.069	
HH-4	$L2_1$	6.061	> 96
	unknown	[a])	

[a]) Cannot be determined.

Table 5. Estimation of lattice strain ε in the Heusler structure from atomic spacing Ni–Al, Ni–Hf and Ni–Ti pairs in B2 and Heusler structures [90T3].

Atomic pair	d^B_{AB} [Å]	d^B_{AC} [Å]	$d^H_{AB=AC}$ [Å]	ε [%]
Ni–Al	2.500		2.624	5.0
Ni–Hf		2.740	2.624	– 4.2
Ni–Al	2.500		2.530	1.2
Ni–Ti		2.611	2.530	– 3.1

Table 4. Compression on Ni–Al–Hf alloys [90T3].

Alloy	*T* [°C]	Yield strength [MPa]	Ultimate strength [MPa]	Ductility [%]
HH-1	RT	1344	1854	4.5
	500	932	1222	6.7
	1000	243 (295)	(304)	> 50 (1.3)
HH-2	RT	2072	2551	0.9
	500	1682	1700	1.0
	1000	282		> 50
HH-4	RT		1036	0
	500		1115	0
	1000	492		> 50

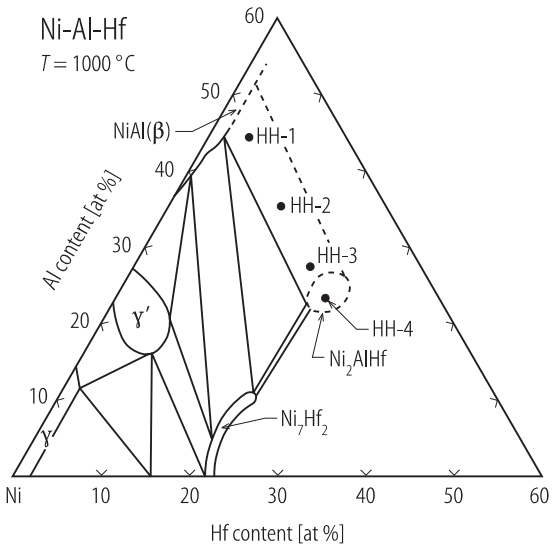

Fig. 20. 1000 °C isothermal section of the Ni-rich corner of the Ni–Al–Hf ternary phase diagram. The solid circles denote the alloys referred to in other figures and tables [90T3].

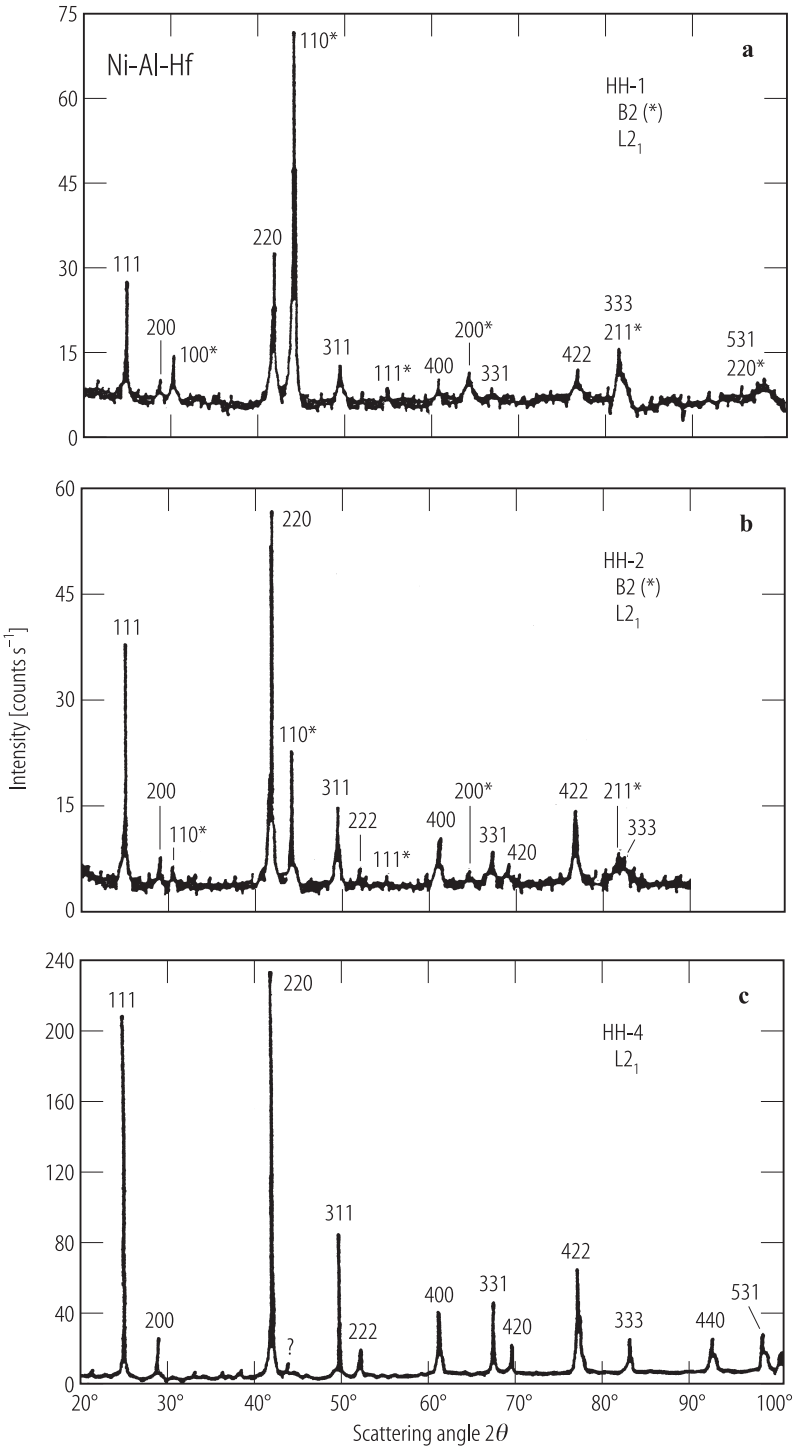

Fig. 21. X-ray diffraction patterns of standard heat treated (1150 °C/1d plus 900 °C/5d in vacuum of (**a**) HH-1, (**b**) HH-2 and (**c**) Hh-4. (See Fig. 20)) [90T3].

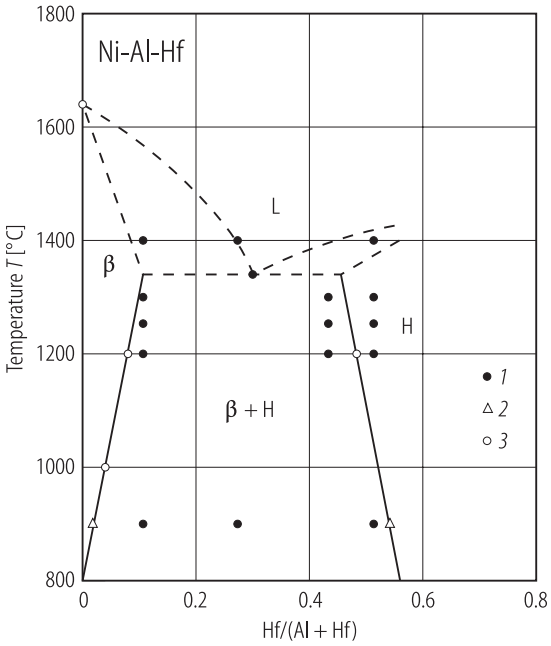

Fig. 22. Estimated phase diagram of (NiAl)(β) - Ni_2HfAl (H) pseudo binary system. *1*: [90T3], *2*: calculated values from volume fraction, *3*: Nash's data.

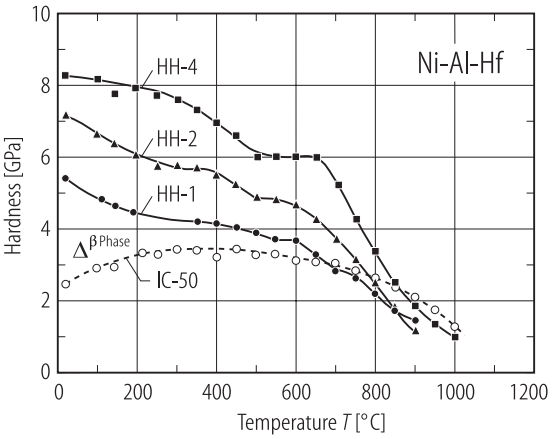

Fig. 23. Change in hardness with temperature of HH-1, HH-2 and HH-4 together with IC-50 (Ni–23.5Al–0.5Hf–B) for comparison. The room temperature hardness of NiAl-β phase is also included [90T3].

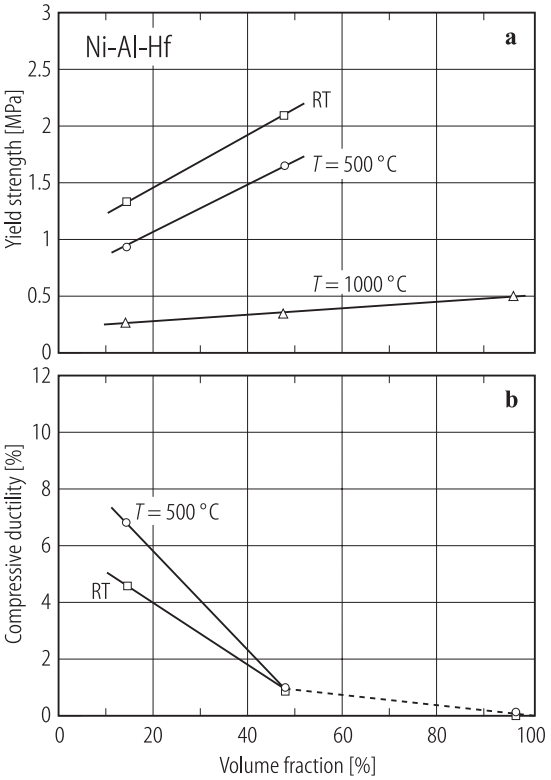

Fig. 24. (**a**) Yield strength and (**b**) compressive ductility of alloys studied as a function of the volume fraction of Heusler phase [90T3]. Ductility of the alloys at 1000 °C is larger than 50 %.

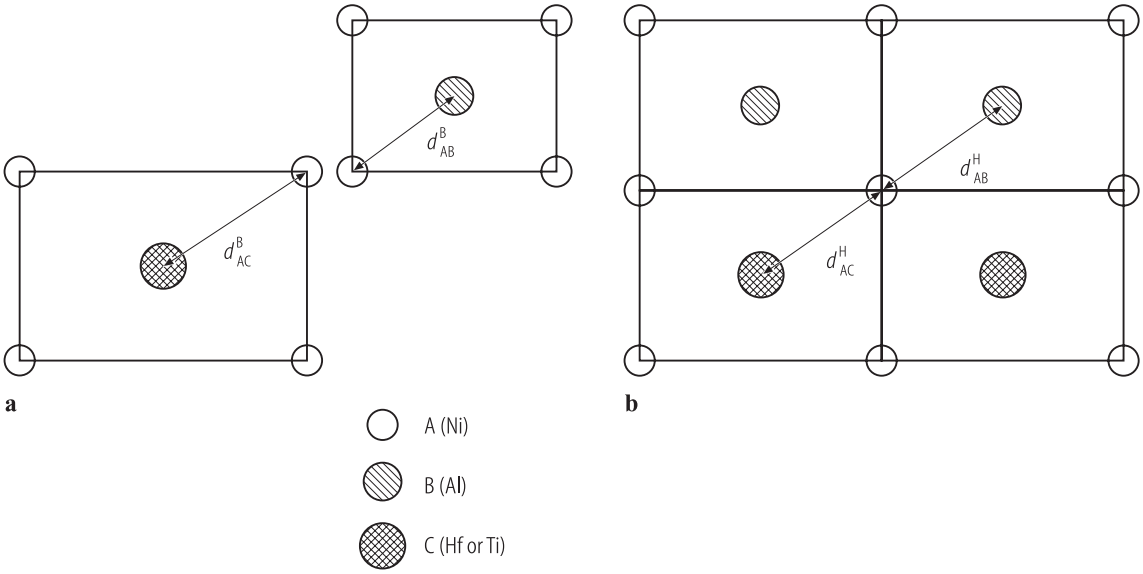

Fig. 25. Schematic illustration of (**a**) B2 structures, AB and AC compounds and (**b**) $L2_1$ structure, A_2BC compound viewing from {110} closed pack plane [90T3].

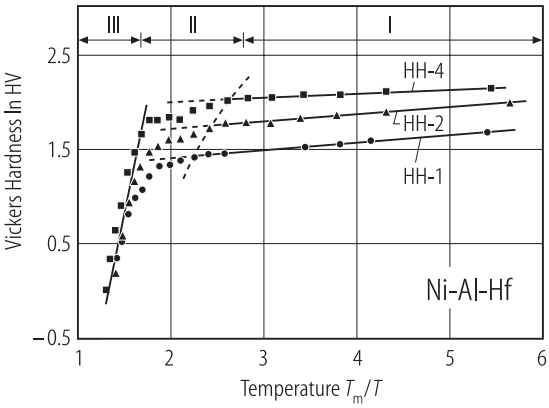

Fig. 26. Hardness HV of HH-1, HH-2 and HH-4 samples as a function of reciprocal temperature (T_m: melting point). Region (I) is the athermal process of deformation; (II) is the transition regime and region (III) is the thermally activated process of deformation [90T3].

Mg–(R)–Ag

Ternary intermetallic phases of several systems where R = La, Ce, Pr, Nd or Sm have been investigated by differential thermal analysis and X-ray diffraction.